Appl. Phys. A 64, 1–6 (1997)

Applied Physics A Materials Science & Processing

Invited paper

Observation of plasma shielding by measuring transmitted and reflected laser pulse temporal profiles

Xianglei Mao, Richard E. Russo*

Lawrence Berkeley National Laboratory, Berkeley, California 94720
(Fax: +01-510/486-7303, E-mail: RERUSSO@LBL.GOV)

Received: 28 August 1996 / Accepted: 17 October 1996

Abstract. Mass ablation rate increases with laser power density following a power law dependence and a significant change occurs at 0.3 GW/cm^2. A reflected laser temporal profile was measured from a brass sample. When the power density is greater than 0.3 GW/cm^2+, the temporal profile changes. The transmitted laser-pulse temporal profile through a glass sample also was measured. When the power density is greater than 0.3 GW/cm^2, the later part of laser pulse becomes truncated. The power density at which the laser temporal profile changes for each case is same as the power density that the mass ablation rate coefficient changes. The ablated mass can absorb incoming laser radiation through inverse Bremsstrahlung. The mass becomes thermally ionized and opaque to the incident radiation, preventing laser light from reaching the surface. A model based on thermal evaporation and inverse Bremsstrahlung absorption was developed. Calculations show that plasma shielding occurs at approximately 0.3 GW/cm^2. The experiments and model suggest that the significant change observed in mass ablation rate coefficient is caused by plasma shielding.

PACS: 81.60Z; 52.40 NK

Inductively coupled plasma-atomic emission spectroscopy (ICP-AES) has been established as a viable technology for studying laser ablation processes at atmospheric pressure [1–14]. The inductively coupled plasma provides a high temperature environment for vaporization, atomization, excitation, and ionization of the ablated mass, spectral emission intensity from the ICP is proportional to the quantity of mass removed by the laser ablation processes. The ICP spectral emission intensity normalized to laser beam area represents the mass ablation rate (mass/(area time)). Previous studies have shown that spectral emission in the ICP exhibits a unique non-linear dependence versus laser power density [12–15]. The ICP/area data versus power density follow two straight lines below and above approximately 0.3 GW/cm^2 for many different sample materials [13], indicating a change in laser ablation mechanisms over this power density region. The mass ablation rate always increases faster in the lower power density region, before the roll-off at approximately 0.3 GW/cm^2.

One possible mechanism to explain the roll-off in mass ablation rate above 0.3 GW/cm^2 is plasma shielding; the laser induced surface plasma becomes optically dense at high power density. The later part of laser pulse energy will interact with the plasma, to be absorbed or reflected. The concept was developed in the early 1960's [16] and several models describing plasma shielding have been presented [17–19]. Wolff-Rottke et. al. drilled a small hole ($< 50\,\mu$m) in polyethylene-teraphtalate samples and measured the temporal pulse shape and energy behind the sample [20, 21]. They found that the laser pulse duration was truncated at higher power density. These experiments demonstrated that the lateral dimension of the plasma was dense enough to cause plasma shielding. Tokarev et. al. measured the reflected temporal profiles of laser pulses from silicon samples [18]. The measurements showed a shorter laser pulse duration after the laser reflected from the surface. These two studies indicate that the plasma interaction with the incident laser beam is important at high laser power density.

In this work, we measured the transmitted and reflected laser pulse temporal profiles versus power density during ablation of glass and brass targets. The reflected data are compared to the mass ablation rate behavior measured in the ICP. A model is proposed to explain this behavior based on thermal evaporation and inverse-Bremsstrahlung heating. From the model, plasma shielding is predicted to occur at approximately the same laser power density that the mass ablation rate measured in ICP rolls-off, and when the reflected and transmitted pulses became truncated.

1 Experimental setup

A diagram of the ICP and reflection measurement system is shown in Fig. 1a. A KrF excimer laser with λ = 248 nm was used for ablation. The pulse duration of the excimer laser is approximately 30 ns. The laser was pulsed at a repetition rate of 10 Hz. The diameter of the beam was reduced by using a 6 mm diameter aperture, then focused into the ablation sample chamber using a plano-convex UV-grade quartz lens (f = 200 mm). The laser beam spot size at the sample

* Author to whom correspondence should be addressed.

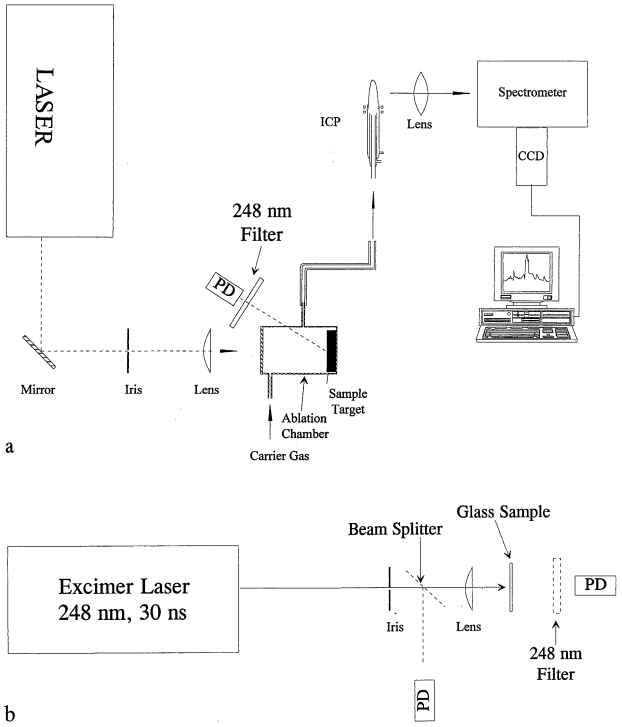

Fig. 1. a Diagram of the experimental laser ablation sampling ICP-AES system with photodiode (PD) detector for measuring reflected light. **b** Diagram of transmission experimental setup

surface was varied by changing the lens to sample distance. The energy of the excimer laser is 25 mJ after the aperture for most of the experiments. The laser ablation chamber was mounted on an xyz micrometer translation stage so the laser spot at the sample surface could be changed after each measurement. A photodiode was placed in front of the sample to record the reflected laser pulse, with a 248 nm band pass filter. The data were recorded for the first laser pulse at each fresh sample surface.

The ICP system was described in previous papers [22,23]. Briefly, the system includes a 2.2 kW RF generator, impedance matching network, and mass flow controllers (Matheson, 8274). The flow rate of Ar plasma gas was 14 L/min and auxiliary gas was 1.0 L/min. The carrier gas (0.2 L/min) transports the ablated mass directly into the central channel of the ICP torch. The measurement system consists of a monochromator (Spex industries; 270M) with a 1200 grooves/mm holographic grating and an entrance slit width of 12.5 μm, and a Peltier cooled, charged-coupled device (CCD) detector with 512×512 pixels (EG & G PAR, OMA VISION). The spectral emission from the ICP was imaged using a quartz lens (5 cm focal length) onto the monochromator. This spectrometer simultaneously measures a 30 nm wavelength range. The size of the CCD is 1x1 cm. The data from the CCD was digitized and transferred to a microcomputer. The samples consisted of small discs (20 mm diameter and 1 mm thickness) of brass. The composition of the brass is approximately 36% Zn and 64% Cu measured by Energy Dispersive X-Ray Spectroscopy.

The transmission experimental setup is shown in Fig. 1b. A focused laser pulse hits a glass sample. A photodiode with a 248 nm band pass filter is placed in back of the sample to record the transmitted laser pulse duration. Data are recorded for the first laser pulse at each new sample surface location.

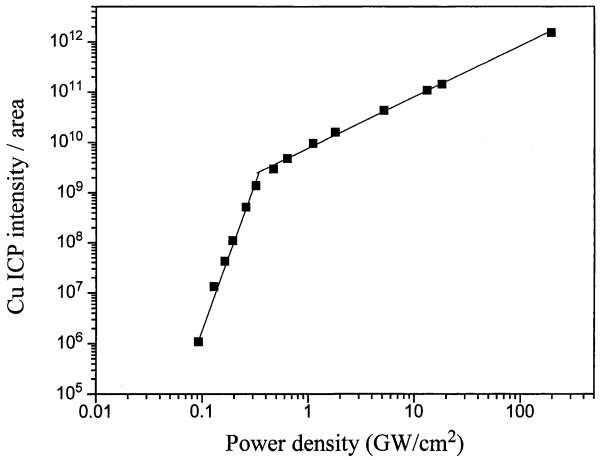

Fig. 2. ICP emission intensity / area versus laser power density showing the two distinct mass ablation rate and roll-off at 0.3 GW/cm^2

2 Results and discussion

The emission intensity in the ICP, normalized to laser beam area versus laser power density is shown in Fig. 2. The ICP/area data exhibit linear behavior with two distinct slopes, below and above approximately 0.3 GW/cm^2, indicating a significant change in the laser ablation mechanisms over this power density region. We observed this behavior for numerous materials with the roll-off occurring at approximately the same power density. One possible explanation for the roll-off is plasma shielding; the later part of laser pulse energy will interact with the plasma, to be absorbed or reflected. A laser plasma interaction can be tested by measuring the reflected or transmitted laser pulse duration.

Figure 3 shows the reflected laser pulse temporal profiles during ablation of brass versus laser power density. The top curve shows the temporal pulse profile of the laser. The temporal profile exhibits multiple-peak structure because of discharge characteristics of the excimer laser. With the power density less than 0.23 GW/cm^2, the reflected profiles were similar to the laser profile. When the laser power density was larger than 0.23 GW/cm^2, the reflected laser pulse duration changes; the later part becomes attenuated. As power density is increased further, the temporal profiles attenuate and truncate significantly. The half width of the reflected laser pulse changes at approximately 0.3 GW/cm^2 (Fig. 4). These measurements support the hypothesis that plasma shielding causes the ablation mechanism to change at approximately 0.3 GW/cm^2 (cf Fig. 2).

These reflection measurements record the laser light penetrating the plasma, reflecting back from the solid sample and through the plasma again. A portion of the laser light will be reflected and scattered from the dense plasma before it reaches the solid sample. The measured reflected light is a combination of these two components (reflected from the solid sample and from the plasma). The pulse duration of laser light penetrating through the dense plasma becomes shorter whereas the portion of light directly re-

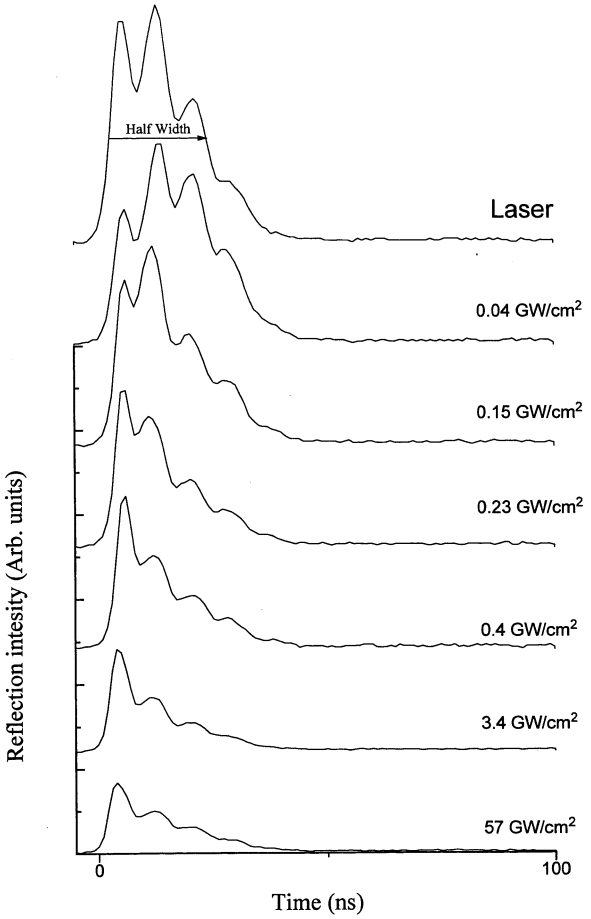

Fig. 3. Reflected laser beam temporal profiles from brass surface at varies power densities. The top curve is the normal excimer laser's temporal profile. The energy of the laser is 25 mJ

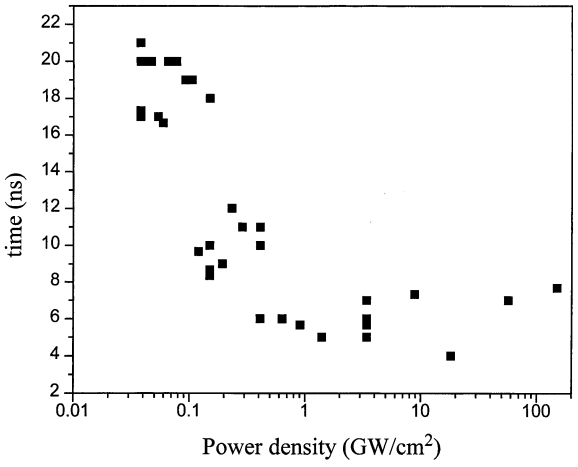

Fig. 4. Temporal half-width of reflected laser pulses versus power density

flected from the plasma surface will maintain the original laser-pulse temporal profile. The density and temperature of the laser induced plasma increases with laser power density. If the plasma electron density reaches a critical level (approximately $1.6 \times 10^{22}/\mathrm{cm}^3$ at 248 nm), the plasma reflectivity can approach one [24]. Therefore, at high power density, the measured reflected laser pulse duration will follow the original profile. The light reflected from the sample

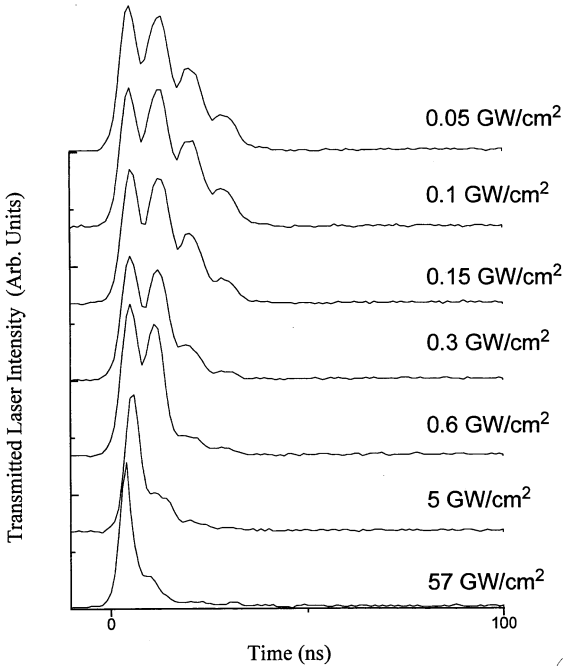

Fig. 5. Transmitted laser beam temporal profiles through a glass sample at varies power densities

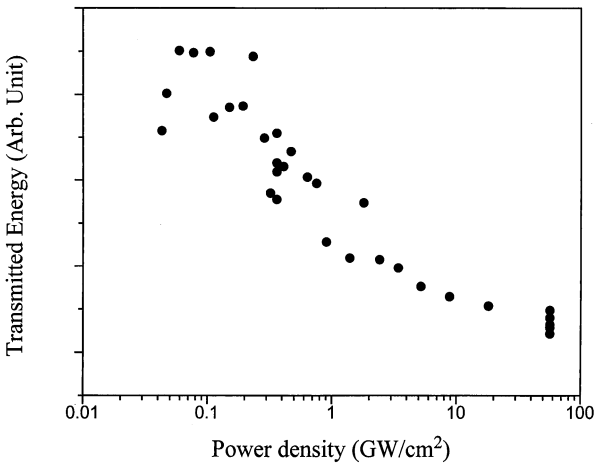

Fig. 6. Integrated laser energy transmitted through the laser induced plasma and glass versus power density

surface has a different temporal profile than the light reflected from the plasma, making interpretation of the results complex. To compliment these reflection measurements, a transmission measurement approach also was employed to monitor plasma shielding. A glass sample was used for these transmission experiments. A small portion of the 248 nm laser energy penetrates through the glass and is recorded by a photodiode with a 248 nm band pass filter. The transmitted laser temporal profiles versus laser power density are shown in Fig. 5. The temporal profiles of the transmitted laser pulse is similar to the original laser pulse until the power density reaches approximately $0.3\,\mathrm{GW/cm}^2$. When the power density is greater than $0.3\,\mathrm{GW/cm}^2$, the pulse width becomes shorter. The transmitted energy can be calculated by integrating the laser intensity temporal profile with time. The data in Fig. 6 shows the transmitted laser energy versus power density;

the transmitted energy decreases when laser power density reaches 0.3 GW/cm^2; the laser energy can be absorbed and/or reflected by the plasma. From previous studies of laser ablation using ICP-AES, the roll-off power density was found to be almost independent of the target material [13]. The truncation of laser pulse duration beginning at 0.3 GW/cm^2 suggests that plasma shielding may be influencing the transmission.

Laser ablation involves complex processes, with many simultaneous mechanisms influencing the amount and composition of the vapor. The surface temperature increases and neutral atoms are evaporated as laser light is absorbed by the target. Electrons are emitted from the surface. These electrons can gain energy from the laser light during collision with atoms and ions (inverse Bremsstrahlung process). Ionization processes begin when the kinetic energy of the electrons is higher than the ionization potential of evaporated atoms. The laser induced plasma above the surface can shield portions of the laser beam during the pulse. To support the hypothesis that mass ablation rate roll-off and truncation of the laser pulse is caused by plasma shielding, a preliminary model with thermal evaporation and inverse Bremsstrahlung heating was developed [14]. Using this model the laser light transmitted through the plasma can be calculated.

The ablated vapor is described by three components: electrons, ions, and neutral atoms with subscripts e, i, and n, respectively.

The energy of electrons is [25, 26]:

$$\epsilon = \frac{3}{2} n_e k_B T_e + n_e k_B \Theta_i \tag{1}$$

where T_e and n_e are electron temperature and density. Θ_i is the ionization potential. The first term is kinetic energy and the second is ionization energy. The energy of particles (ions and atoms) is:

$$\epsilon_p = \frac{3}{2} n_p k_B T_p \tag{2}$$

where T_p and n_p are particle temperature and number density.

Assuming that the electron density and temperature are homogenous in the entire vapor cloud, the change of electron energy should equal to energy absorbed from the laser light minus energy transferred to particles via collision,

$$\frac{\mathrm{d}\epsilon_e}{\mathrm{d}t} = \frac{(1-\exp(-Hk_1))}{H}(1-R)I_0(t) - \frac{3}{2}k_B(T_e - T_p)\nu_{\mathrm{tr}} n_e \tag{3}$$

where $I_0(t)$ is the laser intensity as a function of time, ν_{tr} is the energy transfer frequency, k_1 is the absorption coefficient of the plasma, H is the thickness of the plasma, and R is the reflectivity of the target. At λ = 248 nm, the reflectivity of Cu is 0.34. The reflectivity of Al decreases to zero during the laser pulse after surface melting start [25]. Therefore, we only consider that R is a small value (0.01) in this model. By assuming the plume expands with sonic velocity,

$$\frac{\mathrm{d}H}{\mathrm{d}t} = \sqrt{\frac{\gamma k_B T_p}{M}} \tag{4}$$

where γ is the ratio of C_p and C_v. M is particle mass. The absorption coefficient for inverse Bremsstrahlung can be defined as [26],

$$k_1 = \frac{3.7\times10^8}{\sqrt{T_e}\omega^3} Z^2 \left[\exp\left(\frac{h\omega}{k_B T_e}\right) - 1\right] n_e n_i + \frac{e^2 \nu_c n_e}{\pi m c \omega^2} \tag{5}$$

where ω is the laser frequency, Z is the ionic charge, m is electron mass, e is electron charge, c is light speed, and n_i is number density of ions. The first term in Eq. 5 represents absorption from ions whereas the second term is absorption from atoms. The electron-atom collision frequency ν_c is

$$\nu_c = n_a \sigma_c \sqrt{\frac{8 k_B T_e}{\pi m}} \tag{6}$$

where σ_c is the electron-atom collision cross section and n_a is the density of atoms.

The change of particle energy is equal to the kinetic energy transferred from electrons and the kinetic energy carried by the atoms vaporized from the sample surface. If we assume that the temperature of atoms vaporized from the surface is equal to the surface temperature, then

$$\frac{\mathrm{d}\epsilon_p}{\mathrm{d}t} = \frac{3}{2} k_B T_s \frac{J_v}{H} + \frac{3}{2} k_B (T_e - T_p) \nu_{\mathrm{tr}} n_e. \tag{7}$$

The ionization rate is [26]:

$$\frac{\mathrm{d}n_e}{\mathrm{d}t} = \alpha_i n_a n_e - \beta_R n_i n_e^2 \tag{8}$$

where

$$\alpha_i = C_i \sqrt{k_B T_e} \exp(-\Theta_i / T_e) \tag{9a}$$

and

$$\beta_R = C\left[2\left(\frac{2\pi m}{h}\right)^{3/2}\left(\frac{g_i}{g_k}\right) k T_e\right]. \tag{9b}$$

C_i is an experimental parameter definined from electron ionization cross section data.

For Z = 1,

$$\begin{aligned} n_e &= n_i \\ n_p &= n_i + n_a. \end{aligned} \tag{10}$$

The change in the number density of atoms in the plasma is equal to atoms evaporated from the surface:

$$\frac{\mathrm{d}\left(H(n_a + n_i)\right)}{\mathrm{d}t} = J_v \tag{11}$$

where J_v is the evaporation rate. Assuming thermal equilibrium [27],

$$J_v = P_v(T_s)\sqrt{\frac{M}{2\pi k_B T_s}} \tag{12}$$

where $P_v(T_s)$ is the vapor pressure of the target elements.

$$P_v(T_s) = 1.06\times10^6 \exp\left(-\frac{Lv}{k_B}\left(\frac{1}{T_s} - \frac{1}{T_B}\right)\right). \tag{13}$$

L_v is the heat of vaporization and T_b is the boiling-point temperature.

For brass, J_v will be:

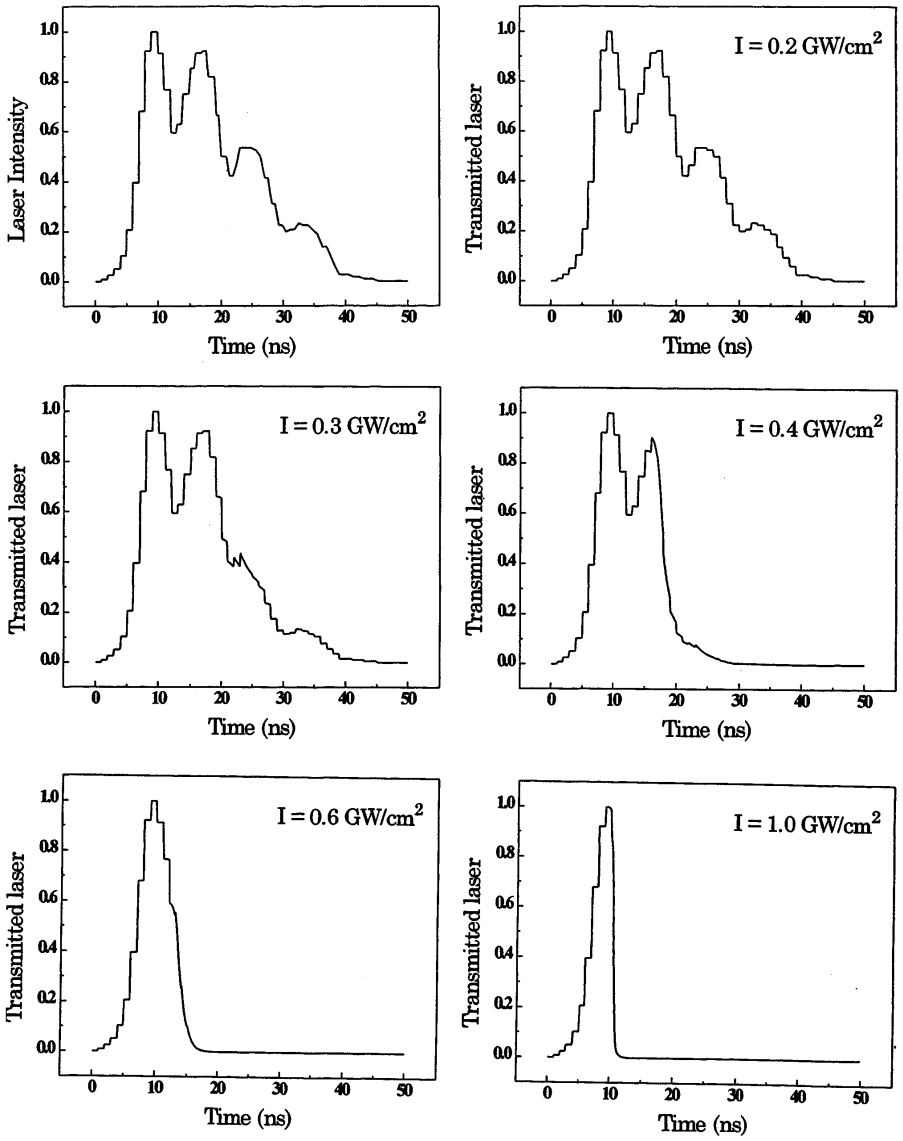

Fig. 7. Transmitted laser temporal profiles calculated from model. Brass optical and thermal parameters are used for calculation. The transmitted laser intensity is normalized

$$J_v = C_{\mathrm{Cu}} P_{v\mathrm{Cu}}(T_s)\sqrt{\frac{M_{\mathrm{Cu}}}{2\pi k_B T_s}} + (1 + C_{\mathrm{Cu}}) P_{v\mathrm{Zn}}(T_s)\sqrt{\frac{M_{\mathrm{zn}}}{2\pi k_B T_s}} \tag{14}$$

where C_{Cu} is the concentration of Cu atoms in the brass alloy. For our sample, C_{Cu} is approximately 0.65.

We have five differential equations (Eqs. 3, 4, 7, 8, and 11) for n_e, n_a, T_e, T_p, H, and T_s and six variables. For surface temperature [28],

$$\frac{\partial T(x,t)}{\partial x^2} = \frac{1}{\kappa}\frac{\partial T(x,t)}{\partial t} \qquad x > X(t), \quad t > 0 \tag{15}$$

$$T(x,0) = T_0$$

$$T(\infty,t) = T_0$$

$$-K\left.\frac{\partial T}{\partial x}\right|_{x=Xt} = I(t) - \varrho L_v \frac{dX(t)}{dt}$$

where K is the thermal conductivity of the target which is assumed to be constant, and ϱ is the density. $X(t)$ is the new surface position during evaporation which is determined by $\frac{dX}{dt} = \frac{1}{\varrho} J_v(T_s)$. By using Eq. 15 we can calculate the surface temperature if we know how much laser light is absorbed. By solving these equations, the transmitted laser light can be calculated at different power densities;

$$I(t) = I_0(t)\exp(-Hk_1) \tag{16}$$

The thermal properties of brass were used to calculate laser temporal profiles transmitted through a plasma (Fig. 7). The model demonstrates that there is no plasma shielding until power density is greater than 0.3 GW/cm^2, at which point the pulse duration begins to truncate. These model data very closely emulate the experimental data measured using both reflection and transmission configurations. When Cu and Zn parameters are used, the calculation shows that the plasma shielding occurs at 0.3– 0.4 GW/cm^2, a close agreement with the experimental measurements [13].

3 Conclusion

ICP-AES emission intensity provides a measurement of mass ablation rate versus laser irradiance at atmospheric pressure. The mass ablation data show a roll off at 0.3 GW/cm^2 using a 30-ns UV laser pulse, which is almost independent of target material. Reflected and transmitted laser temporal profiles become truncated at power density greater than approximately 0.3 GW/cm^2. A preliminary model based on vaporization and inverse Bremsstrahlung shows plasma shielding starts at approximately 0.3 GW/cm^2. Experimental data and the model demonstrate that the percentage of laser pulse energy incident on target decreases with increasing power density. From these data and the preliminary model, plasma shielding is a likely mechanism to explain the roll-off in mass ablation observed in this work.

Acknowledgement. This research was supported by the U.S. Department of Energy, Office of Basic Energy Sciences, Chemical Sciences Division, Processes and Techniques Branch, under Contract No. DE-AC03-76SF00098.

References

1. R. Russo, Appl. Spectrosc. **49**, A14 (1995)
2. S.A. Darke, J.F. Tyson, J. Analyt. Atom. Spectrom. **8**, 145 (1993)
3. L. Moenke-Blankenburg, Spectrochim. Acta Rev. **15**, 1 (1993)
4. R.D. Evans, P.M. Outridge, P. Richner, J. Analyt. Atom. Spectrosc. **9**, 985 (1994)
5. A. J. Walder, I.D. Abell, I. Platzner, P.A. Freedman, Spectrochim. Acta **48B**, 397(1993)
6. L. Moenke-Blankenburg, T. Schumann, D. Gunther, H.M. Kuss, M. Paul, J. Analyt. Atom. Spectrosc. **7**, 251 (1992)
7. N. Furuta, Appl. Spectrosc. **45**, 1372 (1991)
8. Z.W. Hwang, Y.Y. Teng, J. Sneddon, Microchem. J. **43**, 42(1991)
9. W.T. Chan, R.E. Russo, Spectrochim. Acta **46B**, 1471 (1991)
10. X.L. Mao, W.-T. Chan, M.A. Shannon, R.E. Russo, J. Appl. Phys. **74**, 4915(1993)
11. W.T. Chan, X.L. Mao, R.E. Russo, Appl. Spectrosc. **46**, 1025 (1992)
12. A. Fernandez, X. L. Mao, W. T. Chan, M. A. Shanon, R. E. Russo, Analyt. Chem., **67** 2444 (1995)
13. M.A. Shannon, X.L. Mao, A. Fernandez, W.-T. Chan, R.E. Russo, Analyt. Chem. **67**, 4522 (1995)
14. X.L. Mao, W.T. Chan, M. Caetano, M.A. Shannon, R.E. Russo, *Applied Surface Science*, **96-8**, 126–130 (1995)
15. R.E. Russo, X.L. Mao, W.T. Chan, M.F. Bryant, W.F. Kinard, J. Analyt. Atom. Spectrosc. **10**, 295 (1995)
16. J.F. Ready: *Effects of High-Power Laser Radiation*, (Academic Press, Inc., New York, 1971) pp 67–125
17. R.K. Singh, J. of Electronic Materials, **25**, 125 (1996)
18. V. Tokarev, W. Marine, J.G. Lunney, M. Sentis, Thin Solid Films, **241**, 129(1994)
19. V. N. Tokarev, J.G. Lunney, W. Marine, M. Sentis, J. Appl. Phys. **78**, 1241 (1995)
20. B. Wolff-Rottke, J. Ihlemann, H. Schmidt, A. Scholl, Appl. Phys. A, **60**, 13 (1995)
21. J. Ihlemann, A. Scholl, H. Schmidt, B. Wolff-Rottke, Appl. Phys. A, **60**, 411 (1995)
22. M. Caetano, X.L. Mao, R.E. Russo, Spectrochimica Acta, Part B, accepted for publication, (1996)
23. X.L. Mao, R.E. Russo, J. Analyt. Atom. Spectrosc., accepted for publication, (1996)
24. M. von Allmen: *Laser-Beam Interactions with Materials - Physical Principles and Applications* (Springer-Verlag, New York, 1987), pp 16,156.
25. I. Ursu, I.N. Mihaiescu, I. Apostol, M. Dinescu, Al Hening, M. Stoica, A.M. Prokhorov, V.P. Ageev, V.I. Konov, V.N. Tokarev, J. Phys. D: Appl. Phys., **17**, 1315 (1984)
26. R.J. Harrach, Theory for laser-induced breakdown over a vaporizing target surface, Report No. UCRL-52389, Lawrence Livermore Laboratory, University of California, (1987)
27. D.I. Rosen, J. Mitteldorf, G. Kothandaraman, A.N. Pirri, E.R. Pugh, J. Appl. Phys. **53**, 3190 (1982)
28. J.F. Ready, J. Appl. Phys. **36**, 462 (1965)

This article was processed by the author using the LaTeX style file *pljour2* from Springer-Verlag.